Journal of Applied Polymer Science

Studies on thermal degradation and flame retardant behavior of the sisal fiber reinforced unsaturated polyester toughened epoxy nanocomposites

Nagarjuna Reddy Paluvai,[1,2] Smita Mohanty,[1,2] S. K. Nayak[1,2]

[1]Advanced Research School for Technology & Product Simulation (ARSTPS), Central Institute of Plastics Engineering and Technology (CIPET), Chennai, India

[2]Laboratory for Advanced Research in Polymeric Materials (LARPM), Central Institute of Plastics Engineering and Technology (CIPET), Bhubaneswar, India

Correspondence to: N.R. Paluvai (E-mail: nag1987@gmail.com)

ABSTRACT: Unsaturated polyester (UP) toughened nanocomposites were prepared using both sisal fibers and montmorillonite clays. The effect of fibers and Cloisite 30B (C30B) nanoclays on the mechanical properties, thermal stability, flame retardant, and morphological behavior of the UP toughened epoxy (Epoxy/UP) were systematically studied. The chemical structures of Epoxy, UP, and Epoxy/UP systems were characterized using Proton Nuclear magnetic resonance (^{1}HNMR) and Fourier transform infrared (FTIR) spectra. The homogeneous dispersion of nanoclay within the polymer matrix was analyzed using transmission electron microscopy (TEM) and X-ray diffraction (XRD) analysis. Incorporation of sisal fibers and C30B nanoclays within Epoxy/UP system resulted in an increase in the mechanical, thermal, and flame retardance properties. Thermogravimetric analysis (TGA) has been employed to evaluate the thermal degradation kinetic parameters of the composites using Kissinger and Flynn-Wall-Ozawa methods. Cone calorimeter, UL-94, and LOI tests revealed a reduction in the burning rate of the matrix with the addition of fibers and nanoclays. The results showed that the treated fiber reinforced nanocomposites had higher thermal stability and better flame retardant properties than the treated fiber reinforced composites. © 2015 Wiley Periodicals, Inc. J. Appl. Polym. Sci. **2015**, *132*, 42068.

KEYWORDS: blends; clay; composites; fibers; resins

Received 18 August 2014; accepted 3 February 2015

DOI: 10.1002/app.42068

INTRODUCTION

Natural fiber reinforced thermoset composites have been attracting considerable industrial interests during the last decade due to the several advantages such as, high strength-to-weight ratio, low cost, high strength, high modulus, good wear resistance under heavy load which allows them to compete with their synthetic counterparts.[1,2] Natural fibers have several advantages such as biodegradable, non toxic, easy to handle, light weight, low cost, enhanced energy recovery, high toughness, good thermal properties and ease of handling, as compared to the synthetic fibers. Commercially available natural fibers such as banana, cotton, flax, hemp, kenaf, jute, kenaf, palm, silk and silk, have been widely used as reinforcements in polymeric materials.[3,4] Sisal fibers predominantly extracted from the leaf of Agave sisalana plant have enough mechanical strength to withstand several load bearing applications and in particular are readily available.[5] Extensive literature survey indicates sisal fiber reinforced polymeric composites employing various thermoset and thermoplastic matrices.[6–11] However, these fibers have several impediments, such as inherently high hygroscopic characteristics, poor adhesion with the hydrophobic polymer matrix and limited thermal stability during processing which leads to difficulties in fabrication of composites with desired attributes.[12,13] To overcome these issues, surface modifications of natural fibers plays a significant role in improving the interfacial adhesion between the fibers and polymer matrix.[14] Khan *et al.*[5] have studied the effect of different NaOH concentration (0.25, 0.50, 1, 2, 5, and 10%) on sisal fibers and found that nearly 15.8% enhancement in tensile strength was obtained by 2% NaOH treatment. Mishra *et al.*[13] reported that 5% NaOH treated sisal fiber reinforced polyester composite had a better tensile strength as compared to 10% NaOH treated composites. Similarly, several authors have studied the various surface modification techniques such as alkali, acetylation, benzoylation, clay,[7] permanganate, thermal and silane treatment of natural fibers to improve the interfacial interaction with the polymer matrix.[6,15–17]

Epoxy resins are one of the most dominant thermoset materials used in manifold industrial applications ranging from adhesives to composites. These resins exhibit excellent properties such as mechanical strength, thermal stability, chemical resistance, and adhesion. The major drawbacks of the epoxy monomers are brittle in nature. Many efforts have been made to improve the fracture toughness of epoxies, by modifying it with additives such as elastomers, thermoplastics, thermosets and inorganic fillers.[1,18,19] However, to meet the requirements of high-performance applications, it is a prerequisite to modify the epoxy resins with suitable flame retarding materials such as alumina, bromine, inorganic fillers, nitrogen, phosphorus, polyhedral oligomeric silsesquioxanes, polyamide, polyimide, siloxane, and sulphone.[20–22] Various methods are there to raise the flame retardant nature of the epoxy monomers, *i.e.*, (1) additive type flame retardants, which include inorganic particles; (2) reactive type flame retardants which include phosphorus and nitrogen.[18,23,24] These compounds can bring down the high-temperature transfer between the polymer source and a heat source, and suppress the smoke during combustion.[25,26]

Recently, phosphorus-based epoxy monomers reported by Muriel *et al.*[27] for high-performance applications. The phosphorus compounds are halogen free in nature; generating less toxic gasses and smoke. These phosphorus groups are permanently bonded to the epoxy resins and exhibit high fire resistance. Lin *et al.*[28] had developed novel multifunctional phosphorus epoxy monomers and concluded that the flame retardance was found to be more in $C_{12}P_4$ (phosphorus content is 4 wt %) than that of $C_{12}P_2$. In another investigation, advanced naphthalene containing epoxy monomer was prepared by Wang *et al.*[29] It exhibits better flame retardance as well as higher thermal stability than that of the diglycidyl ether of bisphenol-A (DGEBA) epoxy monomer. Similarly, Qiang *et al.*[30] have reported the flame retardant, and smoke suppressed epoxy monomer containing poly (melamine-ethoxyphosphinyl-diisocynate) (PMPC). PMPC is a combination of phosphorus and nitrogen compounds, which helps to reduce the emissions from smoke and poisonous gasses during a fire. In recent years, the use of inorganic particles such as alumina, carbon nanotubes, montmorillonite clay and silica in epoxy monomers are increasing day by day with enhanced properties.[31] Among inorganic fillers, surface modified montmorillonite clays are one of the most common nanoparticles that provide outstanding performance in high-temperature resistance, flame resistance, and electric insulation. These are currently being incorporated into epoxy monomers to produce layered-silicate nanocomposites, which enhance the flame retardance without sacrificing their essential properties.[32,33]

In this study, the sisal fibers and Cloisite 30B clays were used to prepare fiber reinforced UP toughened epoxy nanocomposite, and their effective properties were studied using TGA, UL-94, and Cone Calorimetry. The epoxy monomers have been modified with the addition of unsaturated polyester (UP) resins without diminution of mechanical properties using high pressure mixing (HPM) method. FTIR and ^{1}HNMR were used to characterize the chemical structure of Epoxy, UP and UP toughened epoxy systems. Sisal fibers were treated with alkali and alkali-silane solutions for improving their interfacial adhesion with the Epoxy/UP system. The Kissinger and Flynn-Wall-Ozawa models[34] are applied to explain the thermal stability of the nanocomposites. SEM as well as transmission electron microscopy (TEM) was used to analyze the morphology of the Epoxy/UP, Epoxy/UP/C30B, and their fiber reinforced composite.

EXPERIMENTAL

Materials

DGEBA epoxy resin (Viscosity: 11 ± 2 Pa s and Epoxide equivalent: 189 ± 5 gm/eq), triethylenetetramine (TETA), UP resin (Viscosity: 0.45 ± 0.05 Pa.s and Acid value: 25 ± 3 mg KOH/g), and other reagents such as methyl ethyl ketone peroxide (MEKP- initiator/catalyst) and cobalt naphthenate (accelerator) were supplied by M/s Allied Agencies (Hyderabad, India). Nanoclay, bis(2-hydroxy-ethyl)methyl tallow ammonium (Cloisite 30B) ions purchased from Southern Clay Products (USA). 3-aminopropyltriethoxy silane was procured from Sigma-Aldrich (Bangalore, India). Sisal fibers used in this work were obtained from tribal districts of Kheonjhar (Odisha, India).

Methods

Cone Calorimetry. Cone calorimeter was used to measure the flammability of the samples according to ASTM E1740, using a Fire Testing Technology apparatus with a truncated cone-shaped radiator. The samples with dimensions of 100 mm × 100 mm × 6 mm were exposed to an external heat flux of 50 kW/m^2 at a heating rate of 1°C to 750°C in the pyrolysis zone.

Flammability Studies. The limiting oxygen index (LOI) was analyzed using Atlas HVUL2 according to ASTM D2863. The UL-94 vertical burning test was performed using Atlas HVUL2 instruments according to ASTM D3801. The dimensions of the samples were 130 mm × 13 mm × 3 mm.

Fourier Transform Infrared (FTIR) Spectroscopy. FTIR spectra of samples were recorded using Agilent Cary 630 FTIR spectrometer (USA) with the attenuated total reflectance (ATR) technique.

Nuclear Magnetic Resonance (NMR). The proton nuclear magnetic resonance (^{1}H-NMR) spectra of the Epoxy, UP and Epoxy/UP samples were recorded on a Bruker AVANCE III 500 MHz NMR Spectrometer (Massachusetts, USA). Tetramethylsilane was used as internal standard and $CDCl_3$ as solvent.

Scanning Electron Microscopy (SEM). The surface morphology of the impact tested samples and fiber were performed using a scanning electron microscope (EVOMA 15, Carl Zeiss SMT, Germany). Before analysis, all the fractured surface of samples were coated with a palladium using a sputtering system to eliminate electric charging during SEM analysis.

Thermogravimetric Analysis (TGA). TGA thermograms of samples were obtained using a thermogravimetric analyzer (Q 50, TA Instruments, USA) as per ASTM E 1641-04, samples of ≤ 10 mg were secured from 2.5°C to 600°C at a heating rate of 2.5, 5, 10°C/min in a nitrogen atmosphere, corresponding initial & degradation temperature; % char was noted.

Transmission Electron Microscopy (TEM). The degree of dispersion of C30B clays in the Epoxy/UP resin was investigated using TEM. Samples with a thickness of 85 nm were

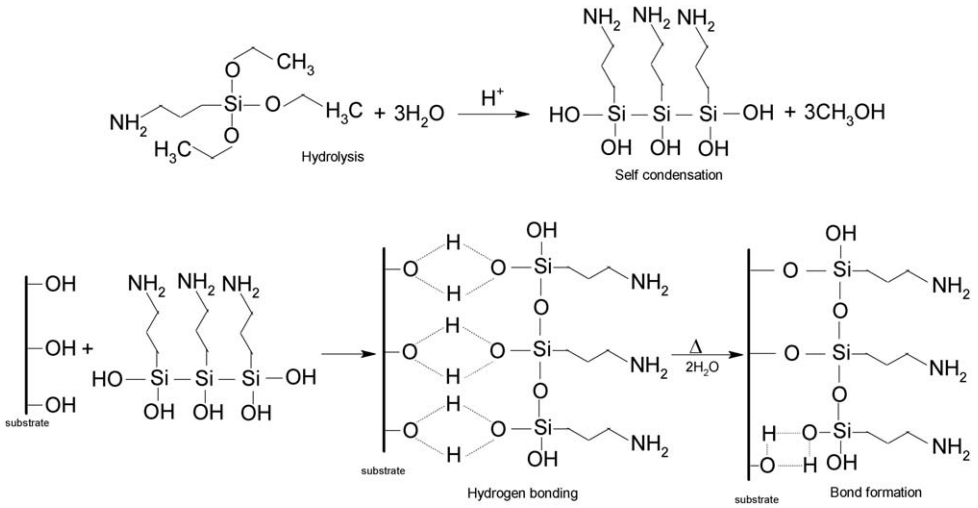

Scheme 1. Reaction mechanism during the silane treatment of sisal fiber.

microtomed using a Leica UC2 Ultra-microtome machine (Wetzlar, Germany) at room temperature. After sectioning, the sections were collected on 200-mesh copper grids. Subsequently, these were examined using a Jeol-2011 Transition Electron Microscope (Peabody, MA) with an accelerating voltage of 200 KV.

X-ray Diffraction (XRD). XRD patterns of samples were recorded at room temperature by monitoring the diffraction angle 2θ from 2 to 10°, at the step size of 0.01° and the scanning speed of 0.05°/min. on a Seifert PTS-3000 diffractometer (Massachusetts, USA). The diffractometer was equipped with a copper target ($k^1/_4$ 1.5405 A°) radiation using a Guinier-type camera employed as a focusing geometry and a solid-state detector. The angle and d-spacing values are calculated through Bragg's law [eq. (1)].

$$nk = 2d \sin\theta \quad (1)$$

where n is an integer, k is the wavelength, θ is the diffraction angle, and d is the interlayer spacing of the crystal.[35,36] Crystallinity index (I_c) of fibers was measured using the Segal empirical method [eq. (2)].[37,38]

$$I_c = \frac{I_{002} - I_{am}}{I_{002}} \times 100 \quad (2)$$

where I_{002} is the maximum intensity of 2θ corresponding to crystalline phase and I_{am} is the maximum intensity of 2θ correspond to amorphous phase in fiber.

Surface Modification of Sisal Fibers

Before surface modification, the fibers were several times washed with ground water followed by detergent diluted solution at 40–50°C to remove the wax and other impurities, and then dried for 24 h.

Alkali Treatment of Sisal Fiber. The fibers of 50 cm length were soaked in 2 wt % NaOH solution at room temperature for 4 h. The NaOH (alkali) treated fibers were washed several times with distilled water containing a few drops of acetic acid to neutralize the excess sodium hydroxide, followed by thorough rinsing with distilled water. The fibers were then dried in the oven at 105°C for 24 h.[5]

Alkali-Silane Treatment of Sisal Fiber. The alkali treated fibers (ATF) were soaked in the 3-aminopropyltriethoxy silane (APTES) solution (the solution contains 6 wt % of silane mixed with ethanol/water in the ratio of 8 : 2) for 1 h. Subsequently, the ethanol–water was drained out and then the fibers were dried in the oven for 2 h at 105°C.[39] The interaction of APTES with natural fibers mainly goes through the succeeding steps,[6,40] presented in Scheme 1.

Fabrication of Fiber Reinforced Composites

Surface modified montmorillonite clays (Cloisite 30B) were utilized for preparation of Epoxy/UP nanocomposites. Before preparing nanocomposites, Cloisite 30B (C30B) clays were dried in an oven at 120°C for 4 h. High-pressure mixing (HPM) method was chosen to disperse the nanoclays into Epoxy/UP resin.[41] Nanoclays was dispersed in acetone and mixed at 1400 rpm for 20–30 min until a wet slurry was obtained. It was mixed with Epoxy/UP (95/5 weight ratio, based on our optimized mechanical data) solution in 200 mL beaker at room temperature with a mechanical stirring for about 4 h to give a homogeneous liquid. Then the mixture was sonicated (Model: LeelaSonic-150, size: 12″ × 6″ × 6″ and capacity: 6.5lt) for about 2 h with pulse mode (15 s on/ 15 s off) to achieve a temperature of 70°C. Heating at this temperature was necessary to remove the residual acetone and to lower the DGEBA viscosity.[42] After mixing the calculated amount of TETA (10 wt %) and MEKP (1 wt % to UP) were added to the above-sonicated mixture. Subsequently, the solution was poured over on the compression mould (Hydraulic press M/s CIPET, India with maximum pressing capacity: 15 tons, maximum piston stroke: ≈50 mm, maximum working pressure: 500 kg/cm^2 and temperature controller from 0 to 500°C with external cooling supply), evenly passed and pushed down with a roller to eliminate the air bubbles, silicon spray used as a mold releasing agent. The mould was kept at room temperature for 24 h, at 80°C for 4 h and post curing was carried out at 110°C for 2 h and at 140°C for 15 min at 70.32 kg/cm^2 pressure in a compression machine. After curing the samples were allowed to cool room temperature and finally

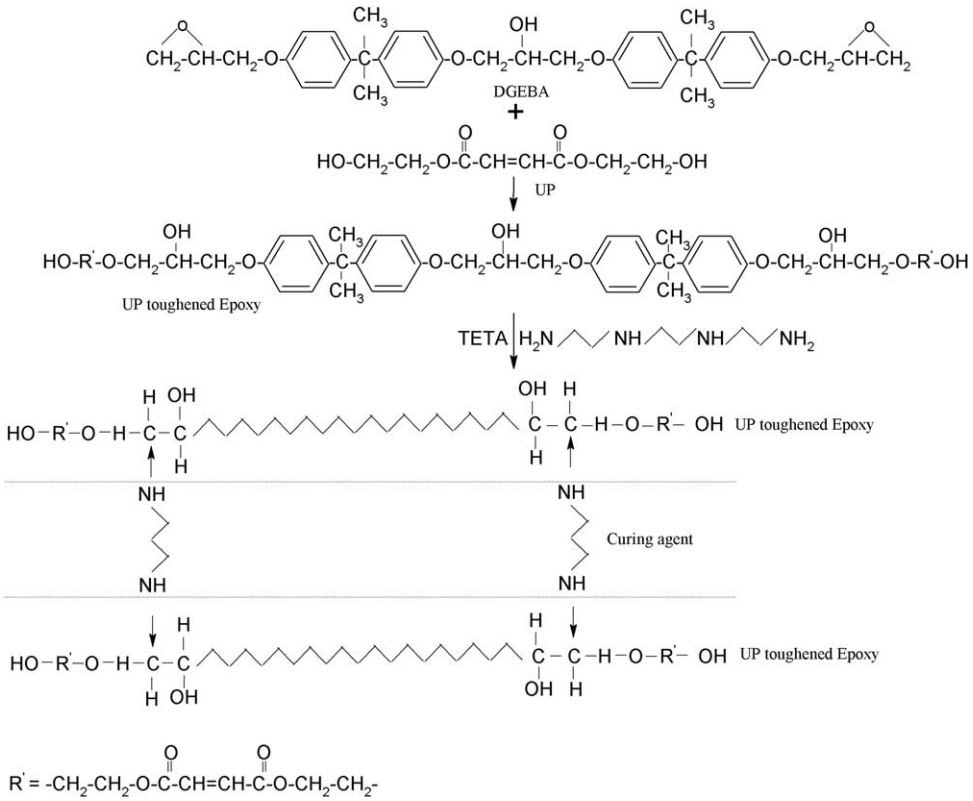

Scheme 2. Possible toughened mechanism between UP and epoxy resins.

removed from the mould and characterized by different properties.[43–46] Similar process parameter was followed for fabricating the Epoxy/UP except the clay mixing into it and sisal fiber reinforced Epoxy/UP nanocomposites obtained by adding 30 wt % alkali-silane treated sisal fiber (ASTF) to the Epoxy/UP/C30B system. The synthesis mechanism of UP toughened epoxy, and its nanocomposites are shown in Schemes 2 and 3.

RESULTS AND DISCUSSION

Fourier Transformation IR (FTIR) Spectroscopy

Characterization of Sisal Fibers. The infrared spectroscopy was used to analyze the effect of the chemical treatments on the surface structure of the fiber and their spectra have been displayed in Figure 1(a). In case the untreated fibers (UTF) the peak at 3337 cm^{-1} reveals the hydroxyl band. After the surface treatment of the fibers, the intensity of the OH band reduced to a frequency of 3300 cm^{-1} for the ATF and 3295 cm^{-1} for the alkali-silane treated fibers (ASTF), respectively which confirms reduced H-bonding in the fibers between the cellulosic hydroxyl groups by the removal of the carboxyl group. It can be seen that the peak at 1732 and 1299 cm^{-1} in the UTF disappeared after the alkali and alkali-silane treatments. The band in the spectrum near 1732 cm^{-1} is attributed mainly to the carboxylic groups corresponding to hemicelluloses. Another band around

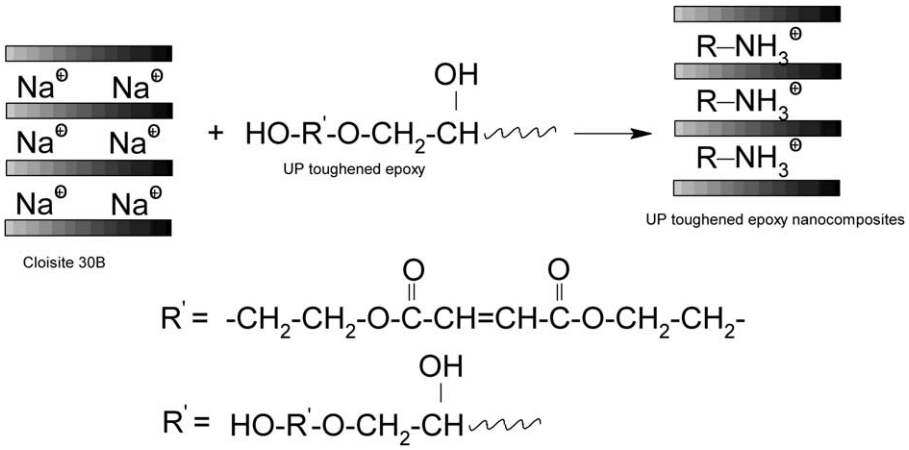

Scheme 3. Synthesis of UP toughened epoxy nanocomposites.

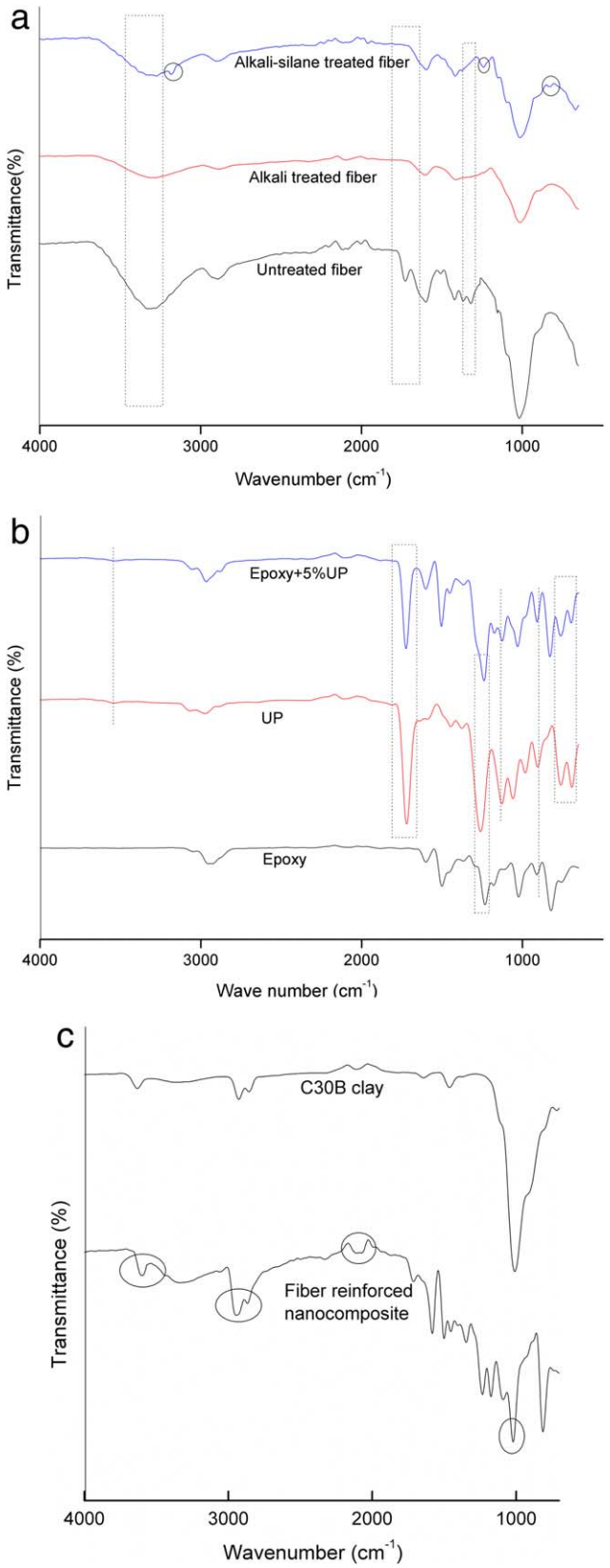

Figure 1. (a) FTIR spectra for untreated and treated sisal fibers, (b) FTIR spectra for UP, Epoxy and UP toughened epoxy, and (c) FTIR spectra of C30 clay and Epoxy/UP/ASTF/C30B system. [Color figure can be viewed in the online issue, which is available at wileyonlinelibrary.com.]

1239 cm^{-1} is attributed to C—O ring of lignin. The results showed that the UTF contained both lignin and pectin that was removed by surface treatments of fibers. In addition, —C—H vibration band at 2899 cm^{-1} in UTF shifts to 2884 cm^{-1} after the treatments. This phenomenon indicated the participation of some free hydroxyl groups in the chemical reaction. The peak at 1430 cm^{-1} corresponds to the absorption of CH_2 group present in cellulose. It has been reappeared at 1415 and 1406 cm^{-1} in the ATF and ASTF. In addition, the peak at 1363 cm^{-1} corresponds to OH in plane bending disappeared upon the chemical treatments. This can also be due to the removal of hemicelluloses. In the case of ASTF, the amine group was introduced to the fibers as demonstrated by the NH_2 stretching band at 3200 cm^{-1}. In addition, strong absorptions related to Si—O and Si—O—Si are observed at 820 and 1239 cm^{-1}, respectively, indicating the reaction between the hydrolyzed silane and the sisal fiber. Chemical modification of sisal fiber removes the hemicelluloses, lignin, and other impurities. These results are in good agreement with the previous reports on the chemical treatments of sisal fibers.[17,44–46]

Characterization of Epoxy, UP, and Epoxy/UP System. Figure 1(b) showed the FTIR spectra of the Epoxy, UP, and Epoxy/UP, respectively. After incorporation of UP within the Epoxy resin, the characteristic peaks appear at 3541, 2968, 1724, 1238, and 1125 cm^{-1} are attributed to the hydroxyl group, methyl (—CH_3) asymmetric stretch, C═O stretching, asymmetric and symmetric C—O—C stretching of aromatic ester, respectively. The spectra were normalized with the absorption band at 1723 cm^{-1} as a reference band. The hydroxyl group for UP at 3541 cm^{-1} and confirmed at 3541 cm^{-1} in the Epoxy/UP system. It confirms the presence of hydrogen bonding between the UP and Epoxy. This was possibly due to the esterification reaction formed between the Epoxy and UP resins. However, the addition of UP into the Epoxy monomer caused the carbonyl group of ester band of the UP resin appear at 1724 cm^{-1} in the Epoxy/UP system, that might indicate the formation of esterification. FTIR spectra of both UP and Epoxy/UP have the absorption around 1260 cm^{-1} indicating an ester group. The absorption bands of UP and Epoxy/UP systems at 1444 and 759 cm^{-1} should attributed to styrene group. It should be noted that C—O—C oxirane group of epoxy peaks at 908 and 823 cm^{-1} are reappeared in the Epoxy/UP due to the toughening mechanism.[47–52]

Characterization of Pure C30B Clay and Epoxy/UP/C30B/Sisal Fiber System. The obtained typical FTIR spectra of C30B and Epoxy/UP/C30B/ASTF system with 1 wt % of C30B clay and 30 wt % of ASTF were shown in Figure 1(c). Characteristic peaks of OH stretching of the Epoxy/UP/C30B/ASTF system were observed at 3400–3273 cm^{-1} which shows a small shoulder due to the reaction between hydroxyl groups of ASTF and amine group of C30B clay with the Epoxy/UP system. A small increase in the peak at 2921 and 2860 cm^{-1} of C30B clay, which can be seen at 2939 and 2865 cm^{-1} in Epoxy/UP/C30B/ASTF correspond to methylene asymmetric and symmetric stretching. Similarly, the band at 1010 cm^{-1} of C30B clay appears at 1019 cm^{-1} in the fiber reinforced nanocomposite spectra. This behavior confirmed the formation of hydrogen bond between

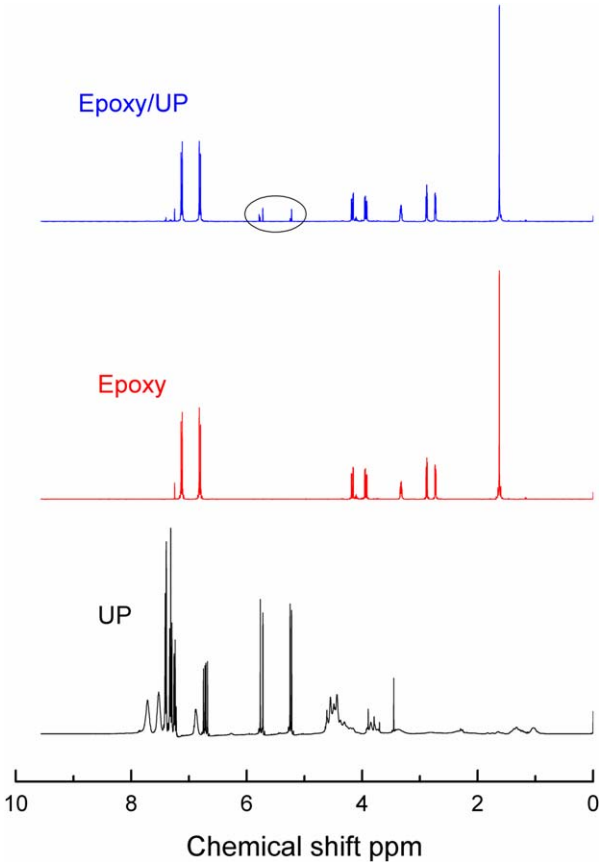

Figure 2. ^{1}HNMR spectra of Epoxy, UP, and Epoxy/UP systems. [Color figure can be viewed in the online issue, which is available at wileyonlinelibrary.com.]

the OH group of the fiber, alkyl ammonium ions of C30B and toughened matrix.[53,54] Further the fiber reinforced nanocomposites also depicted an amine N-H stretch of C30B clay at 3634 cm^{-1} that appeared at 3610 cm^{-1} in case of the Epoxy/UP/C30B/ASTF system. However, the amount of clay present in the nanocomposite system is much less than that of fiber and toughening system. Therefore, the NH bend at 1644 cm^{-1} peak almost disappeared, and the curves become narrower in the fiber reinforced nanocomposite system.

NMR Spectroscopy

The chemical structure of the Epoxy, UP, and Epoxy/UP systems were confirmed by ^{1}HNMR analysis, and their spectrums are shown in Figure 2. The peaks appeared for epoxy resin found to be the presence of a signal at 1.56–1.7 ppm (CH_3), 2.67–2.92 ppm (CH_2 oxirane), 3.25–3.38 ppm (CH oxirane), and 6.75–7.24 (aromatic ring protons). UP spectra of a signal appeared at 0.89–1.5 (propylene glycol), 3.65–4 and 4–4.6 ppm (ethylene glycol), 5.13–5.3 ppm (propylene glycol), 6.65–6.98 (vinyl group), and 7.2–7.9 (phthalate).[55–57] Similarly, Epoxy/UP signals found for propylene glycol at 5.25 and 5.78 ppm and phthalate at 7.3 and 7.4 ppm with the incorporation of UP in the Epoxy monomer. The other peaks of UP disappear due to the amount of UP (5 wt %) added to the toughened epoxy system is much less. It confirmed that the esterification reaction was favorable.[58]

X-ray Diffraction

The XRD spectrum of ASTF, Epoxy/UP/ASTF, C30B nanoclay, Epoxy/UP/C30B, and Epoxy/UP/ASTF/C30B is displayed in Figure 3 and the d-spacing of C30B is calculated by eq. (1). From the data, it is observed that the sharp peak of C30B nanoclay appeared at $2\theta = 4.8°$ with a corresponding d-spacing at 1.8 nm.[59] The Epoxy/UP matrix containing 1 wt % of C30B nanoclay displayed no visible diffraction peak over the entire experimental range of $2\theta = 0$–30, which indicates the exfoliation of clay in the polymer matrix formed by the reaction occurred between epoxy/amine and the clay layers.[60,61] This fact was supported by several authors.[62–64] It also concluded that the nanocomposites synthesized using mechanical mixing followed by ultrasonication showed an exfoliated structure of 1 wt % C30B clay within the Epoxy/UP system which has been further corroborated using TEM analysis. However, a new peak appeared at 18.4° of 2θ represents the amorphous materials in Epoxy/UP/C30B.[65,66] The untreated sisal fiber (UTF) and ASTF have shown two broad peaks at 2θ close to 16.8° and 16.6° which represents amorphous materials, and others at 22.5° and 22.7° of 2θ represents the crystalline materials of fiber, respectively. Earlier studies report similar facts that the diffraction peaks are due to the cellulose crystalline phase and lignin/hemicelluloses/pectin amorphous phase of sisal fiber.[67] The crystalline index of UTF and ASTF were calculated using eq. (2) and the results are summarized Table I. It was observed that surface modification of untreated sisal fiber with the alkali-silane solution, resulted in an increase in the crystalline fraction of cellulose from 62% to 66% due to the partial removal of lignin, hemicelluloses and pectin.[68] Thus, the data suggests that the alkali-silane treatment

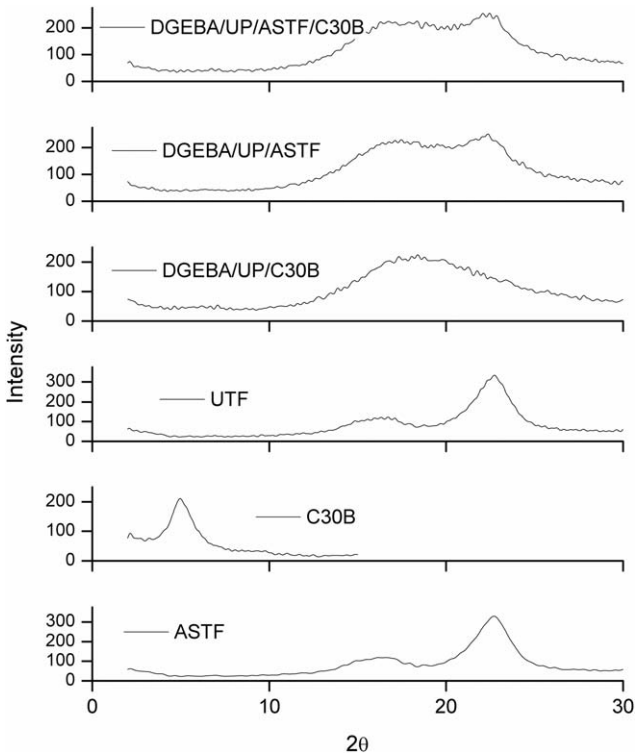

Figure 3. XRD patterns for C30B clay, UTF, ASTF, Epoxy/UP/C30B, Epoxy/UP/ASTF, and Epoxy/UP/ASTF/C30B systems.

Table I. Crystallinity Index of Sisal Fibers

Samples	I_{am}	I_{002}	I_c
UTF	135	358	62.2
ASTF	108	318	66.0

significantly removes the amorphous phase in sisal fiber.[15] The two peaks of ASTF system appeared at 17.4° and 22.36° of 2θ in the fiber reinforced Epoxy/UP composite, and their respective d-spacing values were observed at 0.51 nm and 0.40 nm, respectively. The same peaks shifted to higher 2θ at 18.36 and 22.46 in fiber reinforced Epoxy/UP/C30B nanocomposite system with their respective d-spacing values at 0.48 nm and 0.395 nm, respectively. This phenomenon of the decrease in d-spacing is attributed to an increase in attraction forces between clay platelets and the matrix.[69] It confirms that the formation of fiber reinforced nanocomposites.

Transmission Electron Microscopy

The homogeneous dispersion of the C30B nanoclay layers within the Epoxy/UP, Epoxy/UP/ASTF nanocomposite and Epoxy/UP/ASTF has been analyzed by TEM and their representative micrographs are presented in Figure 4(a–c).[70] The brighter and darker portions in the TEM micrographs are represented the matrix and the C30B nanoclay layers. Figure 4(a) represents the TEM micrograph of Epoxy/UP/C30B system, it shows that the nanoclay dispersed well and randomly penetrates through the Epoxy/UP. It confirms that the exfoliated clay structure within the matrix where the nanoclay patterns are easier to identify because of exfoliation.[71] This is due to the good interactions between the carboxylic ester groups of the polymer and the —OH group of nanoclay. It is also identified from the TEM micrographs; the nanoclays are dispersed of thinner platelets with a thickness of approximately between 30 and 250 nm and disordered randomly in the matrix.[72] This indicates that the 1% C30B nanoclay showed better exfoliation within the Epoxy/UP resin. Figure 4(b,c) shows the TEM micrographs of the ASTF reinforced composite with and without C30B nanoclay. The arrows marks represent the fiber phase in the composite.[7]

Mechanical Properties

The mechanical properties of Epoxy, Epoxy/UP, Epoxy/UP/C30B, Epoxy/UP/ASTF, and Epoxy/UP/ASTF/C30B are shown in Table II. It is evident that by blending of UP resin with epoxy resins significantly increases the tensile, flexural, and impact properties as compared to that of the unmodified resin. The toughened epoxy system at 5wt % UP resin displayed the optimum increases in tensile strength and modulus of 16% and 34%, respectively, as compared with the unmodified resin. A similar rise in the flexural strength and flexural modulus of 19% and 25% was observed. This behavior is due to the esterification occurring between the epoxy and UP, which is attributed to the formation of entangled network structure developed due to unsaturated active sites of polyester toughened epoxy system. Impact strength of 5% UPR with epoxy resins are 37% higher than that of the unmodified resin. The UP resin helps to absorb the impact energy and prevents crack propagation.

The incorporation of 1 wt % nanoclays within the Epoxy/UP matrix increases the mechanical properties including tensile, flexural and impact properties. This is due to the exfoliation of clays within the Epoxy/UP system and the formation of nanocomposites. The Epoxy/UP nanocomposites at 1 wt % clays displayed an increase of 14% in tensile strength, 20% in tensile modulus, 10% in flexural strength, 20% in flexural modulus, and 4% for C30B nanocomposites as compared with the Epoxy/UP matrix. This behavior is due to the good dispersion of nanoclays within the Epoxy/UP matrix, as well as to the good interfacial adhesion between the alkylammonium ion groups of C30B and the Epoxy/UP matrix. The above explanation is well supported by the mechanical property results published by Al-Qadhi *et al.*,[73] which is attributed to the formation of entangled network structure developed due to exfoliated active sites of nanoclays in Epoxy/UP matrix.

The incorporation of 30 wt % ASTF within the Epoxy/UP system increase in tensile strength, tensile modulus, flexural strength, flexural modulus and impact strength to the tune of 83%, 69%, 51%, 145%, and 47% were observed as compared with the Epoxy/UP system. This is due the silane molecule reacts with suitable bonding groups of Epoxy/UP system. This is imputable to the fact that chemical treatments improve the roughness and adhesive characteristics of sisal fiber surface by partial removal of wax, hemicelluloses, and lignin. Thus, chemical reactions occur in sisal fiber, matrix and silane coupling agent. Thereby interfacial properties are improved. The mechanical properties of ASTF reinforced Epoxy/UP nanocomposites increases with the incorporation of 1 wt % C30B clays within

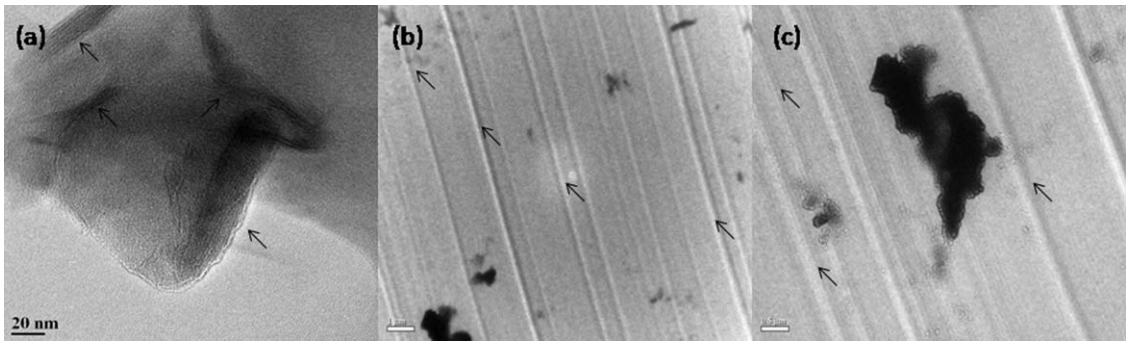

Figure 4. TEM micrographs of (a) Epoxy/UP/C30B system, (b) Epoxy/UP/ASTF, and (c) Epoxy/UP/C30B/ASTF.

Table II. Mechanical Properties of Epoxy, Epoxy/UP, Epoxy/UP/C30B, Epoxy/UP/ASTF, and Its C30B System

Epoxy/UP/C30B/ ASTF composition	Tensile strength (MPa)	Tensile modulus (MPa)	Flexural strength (MPa)	Flexural modulus (MPa)	Impact strength (J/m)
100/0/0/0	56 ± 2	1970 ± 16	100 ± 4	2830 ± 25	151 ± 5
95/5/0/0	65 ± 2	2640 ± 23	119 ± 3	3558 ± 24	207 ± 4
95/5/1	74 ± 1	3175 ± 22	131 ± 3	4267 ± 20	215 ± 3
95/5/0/30	119 ± 2	4476 ± 42	180 ± 3	8740 ± 28	304 ± 2
95/5/1/30	128 ± 2	5047 ± 34	191 ± 2	8978 ± 21	315 ± 3

the Epoxy/UP/ASTF system. It can be seen from Table II, Epoxy/UP/C30B/ASTF system exhibits higher in tensile, flexural, and impact properties than that of the Epoxy/UP/C30B and Epoxy/UP/ASTF systems. The tensile strength, tensile modulus, flexural strength, flexural modulus and impact strength of the Epoxy/UP/C30B system increased from 74 MPa to 128 MPa, 3175 MPa to 5047 MPa, 131 MPa to 191 MPa, 4267 MPa to 8978 MPa, and 215 J/m to 315 J/m with the incorporation of 30 wt % ASTF to it. This is due to the fact of alkali-silane treatment improves the fibrillation of fibers by that silane molecule on the fiber reacts with OH groups of Epoxy/UP system. Thus, interfacial properties are improved by the resultant chemical bonding.

Thermogravimetric Analysis

Thermal Stability. The thermal stability of ASTF, Epoxy/UP, Epoxy/UP/C30B, Epoxy/UP/ASTF, and Epoxy/UP/ASTF/C30B as a function of temperature from 25 to 600°C at 2.5°C/min were examined using TGA analysis (Figure 5). Further, the weight loss at 20%, 60%, and the char residue of all samples has been reported in Table III. The ASTF samples exhibited a higher thermal decomposition temperature up to 240°C where the samples showed thermally stable characteristic, and the mass loss in the sample was relatively small. Beyond 300°C, the samples exhibited a drastic loss in mass which is due to decomposition of cellulose and hemicelluloses. Above 345°C, degradation occurs as a result of delignification of fibers. As can be observed from the Table III, the alkali-silane treatment was effective in improving the thermal stability of the sisal fibers. With the incorporation of 1 wt % C30B nanoclay within the Epoxy/UP systems showed improvements in thermal stability as compared to the Epoxy/UP system.[74] This is due to an increase in the effective cross-linking density in the presence of amine groups in the nanoclay that further acts as a catalyst for the Epoxy/UP system.[75] In the case of Epoxy/UP/ASTF system, the initial weight loss up to 243°C indicates the removal of moisture and other volatiles from the fiber in the composites. The weight loss from 243 to 400°C is primarily due to degradation of the composites. The thermal stability increases with the incorporation of treated sisal fibers into the Epoxy/UP. The weight loss at 60% of Epoxy/UP increases from 371 to 388°C (shown in Table III) with the incorporation of ASTF within the matrix. The decomposition temperature increased in case of ASTF reinforced Epoxy/UP/C30B system, which further confirms strong interfacial balance due to the establishment of hydrogen and covalent bonds. Further, the char residue in case of Epoxy/UP/ASTF system increased from 2.9 to 5.1% with the addition of C30B nanoparticles to it, which additionally confirmed improved flame retardance of the system. The char residues at 600°C of the sample Epoxy/UP/C30B, Epoxy/UP/ASTF and Epoxy/UP/ASTF/C30B are as 3.2 wt %, 2.9 wt %, and 5.1 wt %, respectively, which are improved significantly as compared with that of Epoxy/UP. Thus, it can be seen that the incorporation of C30B clays and ASTF can promote the char formation layer thereby improving its thermal stability.

Kinetics of Thermal Decomposition. The DTG curves of Epoxy/UP, Epoxy/UP/C30B, Epoxy/UP/ASTF, and Epoxy/UP/ASTF/C30B systems at heating rates of 2.5, 5, and 10°C/min are shown in Figure 6(a–d). The thermal decomposition data has been presented in Table IV. The thermal decomposition process of all samples is composed of two main steps as shown in Figure 6(a–d). During the first stage of thermal oxidative degradation process occurs to the degradation of cross-linked Epoxy/UP matrix. The second stage is mainly due to the further oxidative decomposition of previous formed char residue. These findings are correlated with earlier studies reported by several authors.[23,77,78] Two kinetic models proposed by Kissinger and Flynn-Wall-Ozawa were used to obtain the activation energy (E). According to the Kissinger method, from eq. (3):

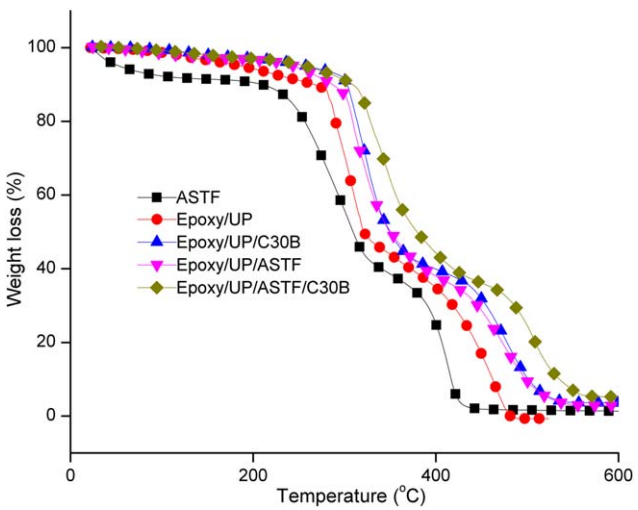

Figure 5. TGA thermogram curves of ASTF, Epoxy/UP, Epoxy/UP/ASTF, Epoxy/UP/C30B and Epoxy/UP/ASTF/C30B systems at a heating rate of 2.5°C/min. [Color figure can be viewed in the online issue, which is available at wileyonlinelibrary.com.]

Table III. Thermogravimetric Data of ASTF, Epoxy/UP, Epoxy/UP/C30B, Epoxy/UP/ASTF, and Its C30B System

Samples	Weight loss 20%	Weight loss 60%	Char yield (%) at 600°C
ASTF	256	340	1.4
Epoxy/UP	290	371	0
Epoxy/UP/C30B	312	493	3.2
Epoxy/UP/ASTF	308	388	2.9
Epoxy/UP/C30B/ASTF	328	417	5.1

$$-\ln\left(\frac{\beta}{T_{max}^2}\right)=\frac{E}{RT_{max}}-\ln\left(\frac{AR}{E}\right) \quad (3)$$

where T_{max} is the peak temperature decomposition rate, β is the heating rate, E is the activation energy, A is pre-exponential factor, and R is the universal gas constant (8.314 J/mol K). The activation energy could be calculated from the plot of an approximately linear relationship between $\ln(\beta/T_{max}^2)$ versus $1/T_{max}$ with the correlation of experimental data as shown in Figure 7. The activation energy obtained for Epoxy/UP, Epoxy/UP/C30B, Epoxy/UP/ASTF and Epoxy/UP/C30B/ASTF systems were 166, 169, 179, and 198 KJ/mol, respectively.

The activation energy changes throughout the entire reaction also observed by Ozawa-Flynn-Wall model. According to the Ozawa–Flynn–Wall analysis, from eq. (4):

$$\log\beta=\log\left[\frac{AE}{g(\alpha)R}\right]-2.315-\frac{0.4567E}{RT_{max}} \quad (4)$$

where $g(\alpha)$ is a conversion dependent function, and other parameters are the same as described earlier. To determine the corresponding activation energy at each degree of cure, a plot of $\log\beta$ versus $1/T_{max}$ was drawn at each heating rate as shown in Figure 8. The resulting slope indicates the activation energy. The activation energy obtained for Epoxy/UP, Epoxy/UP/C30B, Epoxy/UP/ASTF, and Epoxy/UP/C30B/ASTF systems were 168, 172, 180, and 201 KJ/mol, respectively. These values revealed that the surface modified sisal fiber and clay increased the thermal stability of Epoxy/UP system to a greater extent. The activation energies of the composites obtained from the Flynn–Wall–Ozawa Model was higher than that of the Kissinger Model.

Flame-Retardant Properties

LOI Measurements. The LOI is the tendency of a material to sustain a flame, by passing oxygen and nitrogen mixture over a burning specimen. As shown in Table V, the LOI increases from 20% to 24% with the addition of the Cloisite 30B nanoparticles into Epoxy/UP system. This may be due to the higher

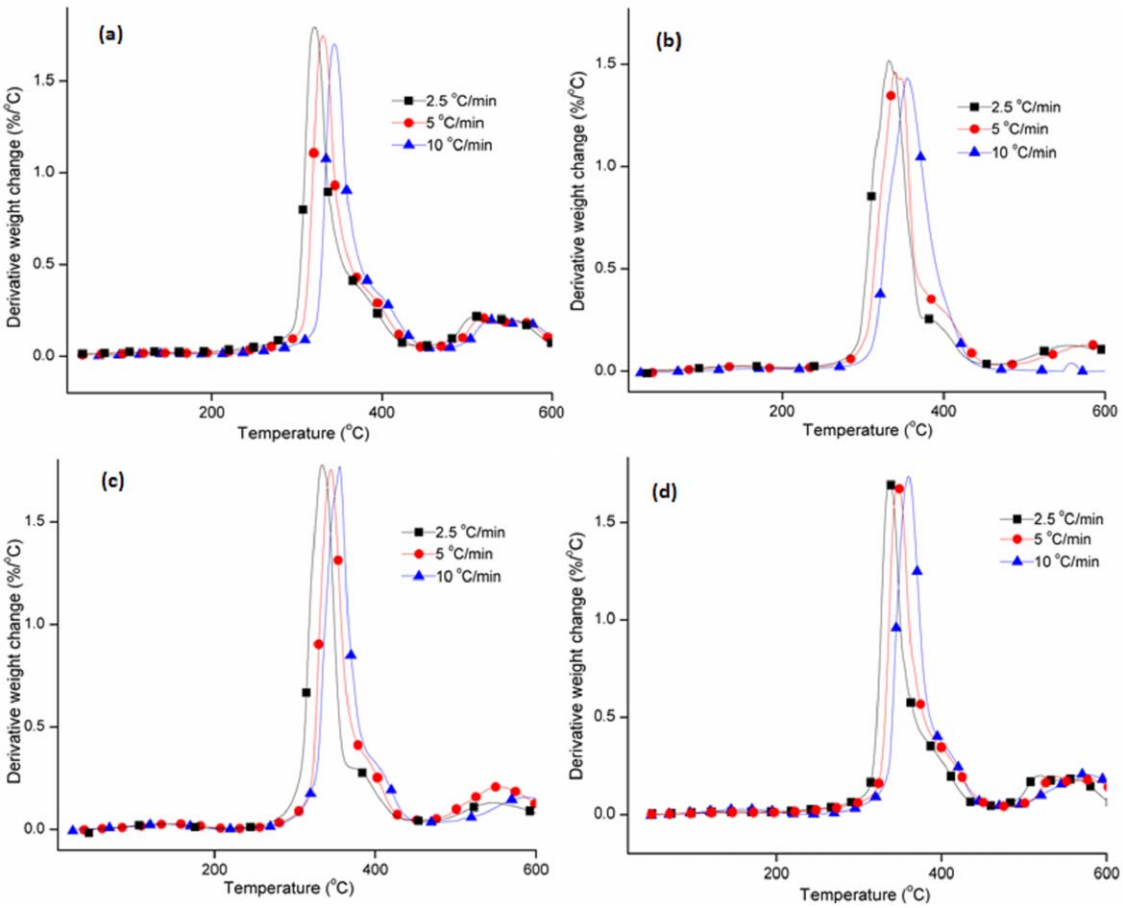

Figure 6. (a–d) DTG thermogram curves of Epoxy/UP, Epoxy/UP/C30B, Epoxy/UP/ASTF and Epoxy/UP/C30B/ASTF systems at a heating rate of 2.5, 5 and 10°C/min. [Color figure can be viewed in the online issue, which is available at wileyonlinelibrary.com.]

Table IV. Kinetic of Thermal Decomposition Data of Epoxy/UP, Epoxy/UP/C30B, Epoxy/UP/ASTF, and Its C30B System

Heating rate, β (K/min)	Epoxy/UP T_{max}(°C)	Epoxy/UP/C30B T_{max}(°C)	Epoxy/UP/ASTF T_{max}(°C)	Epoxy/UP/ASTF/C30B T_{max}(°C)
2.5	321	330	333	338
5	332	342	344	348
10	345	354	356	359

decomposition temperature for Epoxy/UP/C30B as compared with Epoxy/UP and it forms a thick residue which can act as a protective layer. The results indicate that C30B exhibits flame-retardant effect of Epoxy/UP system. Similarly, the LOI value increases from 20% to 25% with the addition of ASTF to the Epoxy/UP system. This is due to the strong covalent bond formed between the treated fiber and matrix, and Si-O-Si linkage on the fiber acts as good thermal resisting agent to the matrix. However, the LOI value increases from 24% to 27% with the addition of 30wt %. ASTF to Epoxy/UP/C30B system. This may be due to the strong covalent bonds formed between the Si-O-Si linkage on the fiber and alkylammonium ions of clay; Epoxy/UP/C30B system; the char yield also affects the LOI, with a higher value for Epoxy/UP/ASTF/C30B system than that for Epoxy/UP/C30B.

UL-94V Test. The UL-94V results of all types of Epoxy/UP systems are shown in Table V. It can be noted that the Epoxy/UP burned rapidly after ignition and exhibited a V2 rating observed during UL-94V test. As shown in Table V, the flame retardance was better for the Epoxy/UP/ASTF, Epoxy/UP/C30B and its fiber reinforced nanocomposite systems, which were rated as a V1.[76] This may be due to the char forming nature of clay and improved interaction between Si-O-Si groups in fiber and OH groups in nanomatrix. These results indicate that Epoxy/UP/ASTF, Epoxy/UP/C30B and its fiber-reinforced composites shows good flame retardance than that of Epoxy/UP system.

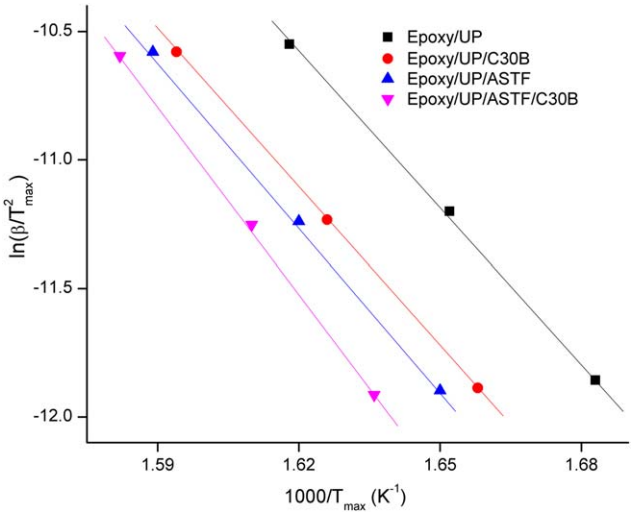

Figure 7. Plots to determine activation energies by the Kissinger Model for Epoxy/UP, Epoxy/UP/ASTF, Epoxy/UP/C30B, and Epoxy/UP/ASTF/C30B systems. [Color figure can be viewed in the online issue, which is available at wileyonlinelibrary.com.]

Cone Calorimeter Analysis. The cone calorimeter has been used to investigate the effects of C30B clay and ASTF on the fire behavior of Epoxy/UP system. The concerned combustion parameters include time to ignition (TTI), peak of heat release rate (p-HRR) and total heat release (THR) are presented in Table VI.[77,78] It can be seen that, with the incorporation of C30B nanoparticles to Epoxy/UP system, the p-HRR and THR values decreases from 829 to 647 kW/m^2 and 141 to 119 MJ/m^2, respectively. This may be due to the viscosity increases with

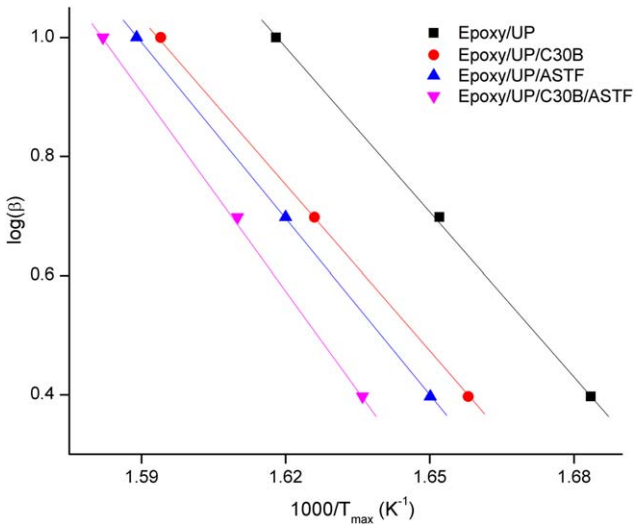

Figure 8. Plots to determine activation energies by the Flynn–Wall–Ozawa Model for Epoxy/UP, Epoxy/UP/ASTF, Epoxy/UP/C30B, and Epoxy/UP/ASTF/C30B systems. [Color figure can be viewed in the online issue, which is available at wileyonlinelibrary.com.]

Table V. Flame Retardant Properties of Epoxy/UP, Epoxy/UP/C30B, Epoxy/UP/ASTF, and Its C30B System

Sample	LOI	UL-94V	Dripping
Epoxy/UP	20	V-2	Yes
Epoxy/UP/1 wt % C30B	24	V-1	No
Epoxy/UP/ASTF	25	V-1	No
Epoxy/UP/1 wt % C30B/ASTF	27	V-1	No

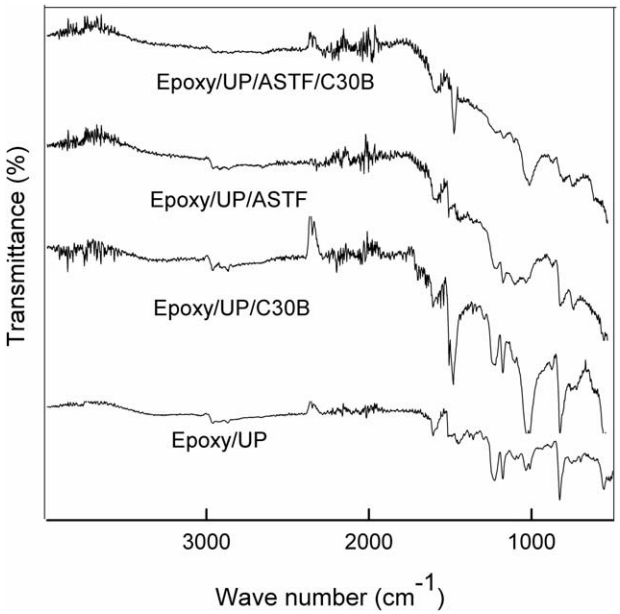

Figure 9. FTIR spectra for char residues of Epoxy/UP, Epoxy/UP/C30B, Epoxy/UP/ASTF, and Epoxy/UP/ASTF/C30B.

Table VI. Cone Calorimeter Data of Epoxy/UP, Epoxy/UP/C30B, Epoxy/UP/ASTF and Its C30B Samples

Samples	TTI (s)	Peak HRR (KW/m^2)	THR (MJ/m^2)
Epoxy/UP	61	829.2	141.7
Epoxy/UP/1 wt % C30B	66	647.2	119.5
Epoxy/UP/ASTF	65	610.9	110.8
Epoxy/UP/1 wt % C30B/ASTF	64	583.3	104.3

the addition of C30B nanoparticles to the Epoxy/UP system, which increases the char formation and increases the resistivity towards flame. Similarly, with the addition of C30 clays to the Epoxy/UP/ASTF, the p-HRR and THR further decreases from 610 to 583 kW/m^2 and 110 to 105 MJ/m^2, respectively. These can be further correlated with the UL-94V and LOI tests, which is attributed to the formation of strong Si-O-Si bonds on the fiber surface, which further protects the C30B clay from fire. Therefore, an improved flame retardant properties can be obtained by the decreased p-HRR and THR.

Residue Characterization

To understand the thermal stability of the Epoxy/UP and its hybrid system, the char residue was analyzed by FTIR spectrometry. As evident from Figure 9, the major peaks corresponding to the water (4000–3400 cm^{-1}), hydrocarbons (3100–2600 cm^{-1}), carbon dioxide (2420–2240 cm^{-1}), carbon monoxide (2240–2040 cm^{-1}), carboxyl and carbonyl functional groups (1800–1600 cm^{-1}), aromatic ring (1600–1250 cm^{-1}) and aromatic-aliphatic compound (1250–1100 cm^{-1}) were observed. Similar facts were also found by several authors.[79–82] As observed from TGA analysis, the char residue for the composites is higher than the Epoxy/UP system, which is due to the water released from the composite. The char residue mainly composed of phenol, compounds containing CH/CH$_2$/CH$_3$ group, carbonyl and aromatic ring. Later, the alkylammonium ions of organoclay bands appear in the Epoxy/UP/C30B and its ASTF system at 1487-1477 cm^{-1} (N-H bending vibration). Taking into account that the degradation behavior is complicated in case of C30B systems than the Epoxy/UP/ASTF and Epoxy/UP system.[83] This is because of C30B nanoparticles enhance carbonaceous char formation by catalytic effect of the clay. At higher temperature, the C30B clay degrades to form acidic protons on the clay layer which further act as heat transfer medium in the condensed phase and stimulate the formation of a char and protecting from volatilizing the matrix, resulting in improvements in the flame retardance of the matrix.[84–86]

Scanning Electron Microscopy

SEM micrographs of UTF, ATF, and ASTF are shown in Figure 10(a–c). It is noted that in case of UTF, there are traces of impurities along the longitudinal surface of the fiber. As can be seen from the Figure 10(b,c), the chemical treatment tends to remove wax and other essences on the fiber surface. The ATF sample was displayed fibrillation and a coarser morphology, which is clearly visible from the microporous structure. Unlike the UTF, the ASTF showed a rough surface due the removal of hemicelluloses and pectin groups that render uniform arrangement of the less dense and rigid fibrils in the tensile direction. Similar phenomenon was observed in the case of ASTF, which demonstrated the presence of macrospores, fibrillation as well

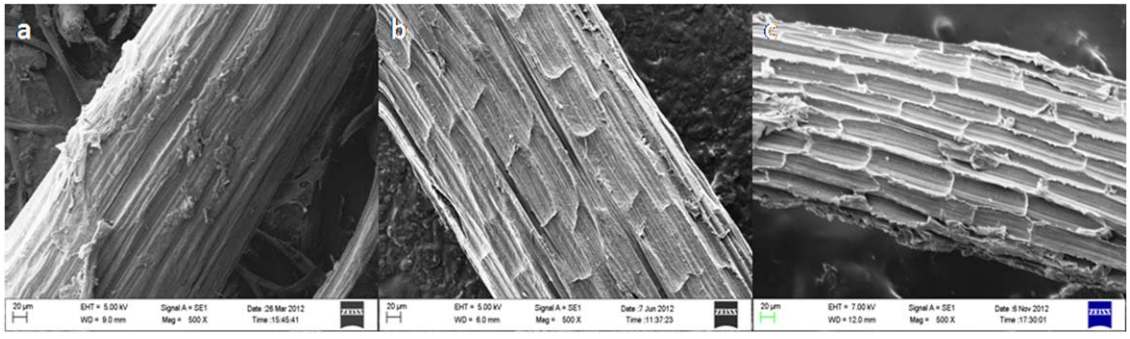

Figure 10. SEM micrographs of (a) untreated, (b) 2% alkali treated, and (c) alkali-silane treated fibers. [Color figure can be viewed in the online issue, which is available at wileyonlinelibrary.com.]

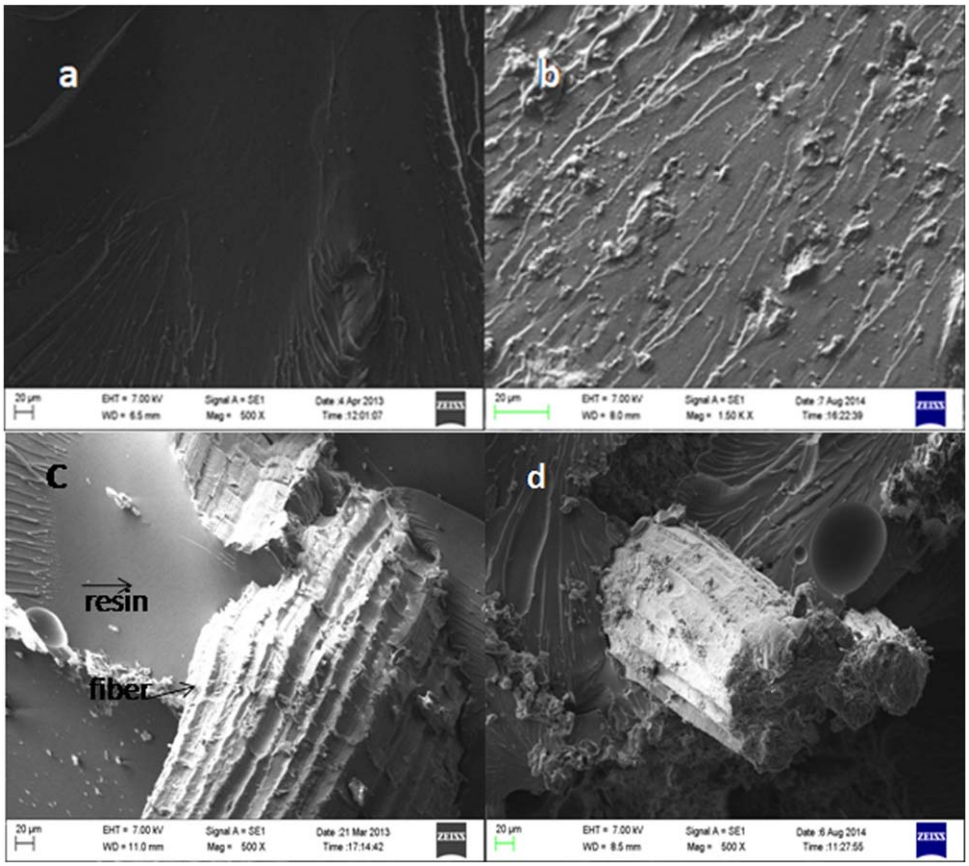

Figure 11. SEM photographs (a) Epoxy/UP, (b) Epoxy/UP/C30B, (c) Epoxy/UP/ASTF, and (d) Epoxy/UP/ASTF/C30B. [Color figure can be viewed in the online issue, which is available at wileyonlinelibrary.com.]

as rougher fiber surfaces. It is assumed that the moisture in the fiber hydrolyzes the silanes to form silanols, which finally forms covalent bonds or H-bonds with the OH group of sisal fiber.[5,87,88] These results concluded that the chemical modification of sisal fiber improves the surface characteristics such as wetting, adhesion, surface tension, and porosity.

SEM micrographs of impact fractured surface of Epoxy/UP, Epoxy/UP/C30B, Epoxy/UP/ASTF, and Epoxy/UP/ASTF/C30B were depicted in Figure 11. From Figure 11(a), it is observed that the miscible characteristic of the Epoxy/UP system resulted in a smooth morphology at the fractured surface. From the micrographs of Figure 11(b), it observed that the ductile nature of the system increases as with the addition of 1 wt % C30B clay to the Epoxy/UP system. However, the fracture surface of Epoxy/UP/C30B become rough thus indicating the improved impact strength.[46,49,89] The fractured surface of Epoxy/UP/ASTF system showed pull out of fibers along with a resin matrix adhering to the fiber, as shown in Figure 11(c). This indicates

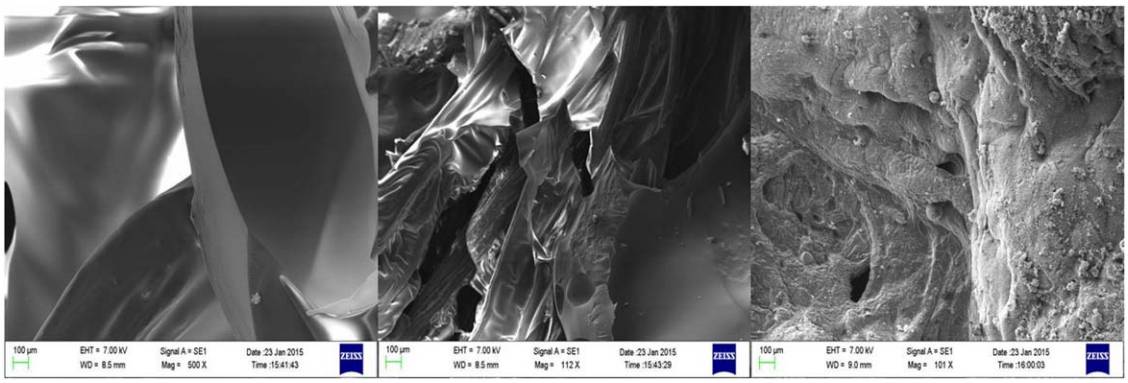

Figure 12. Charred SEM micrographs (a) Epoxy/UP, (b) Epoxy/UP/ASTF, and (c) Epoxy/UP/ASTF/C30B. [Color figure can be viewed in the online issue, which is available at wileyonlinelibrary.com.]

strong adhesion at the interface between the alkali-silane treated fiber and the matrix. The micrograph of fractured Epoxy/UP/ASTF/C30B [shown in Figure 11(d)] indicates that the strong adhesion between the alkali-silane treated fiber and Epoxy/UP/C30B system, which reduces the individual fiber pullout along the existence of cracks at the broken surface.

The SEM micrographs of the residue char after cone calorimeter studied of Epoxy/UP and Epoxy/UP/ASTF and Epoxy/UP/ASTF/C30B systems is presented Figure 12. It can be observed from Figure 12(a), the char of Epoxy/UP is smooth and continual, which means a rapid volatilization at the surface of the matrix. Figure 12(b) shows that the surface of the char of Epoxy/UP/ASTF is easily damaged and weak, which could not effectively protect the alkali-silane treated fiber from fire.[90] Figure 12(c) shows that the surface of the char of Epoxy/UP/ASTF/C30B is continuous and compact. It is possible due to the nanoparticles moved forward to the surface of the matrix caused by the volatile products and the tightly cladded by the char layer. This indicates that the presence of the catalytic effect of nanoparticles can insulate the transfer of heat and promote the char formation, thus improving the flame retardance and reducing the heat release rate of the matrix.[18,91] This is in accordance with the TGA data which confirmed that the char residue of Epoxy/UP/ASTF/C30B system exhibited higher thermal stability than that of Epoxy/UP/ASTF system.[78,92]

CONCLUSIONS

The effect of surface modified sisal fibers and clay on the thermal degradation and flame retardant behavior of UP toughened epoxy system was studied. The FTIR and ^{1}HNMR spectroscopy confirmed that the toughening reaction between UP and epoxy. The XRD curves and TEM micrographs revealed the dispersion of C30B nanoclays within the Epoxy/UP system. From TGA analysis, it concluded that the Epoxy/UP/ASTF/C30B system exhibit higher thermal stability than the other systems. The alkali-silane treated fiber and C30B nanoclay influenced on the thermal decomposition of Epoxy/UP system. The activation energy (E_a) for Epoxy/UP/ASTF/C30B system obtained by Flynn-Wall-Ozawa equation (201 KJ/mol) showed higher than that of the Kissinger equation (198 KJ/mol), respectively. However, the increased E_a is indicating that increments in the thermal stability of the matrix. The LOI value risen from 22 to 27 and the UL-94 changed from V-2 to V-1 with the addition of ASTF and C30B nanoclays to the Epoxy/UP system. It indicates that the nanoclay particles and treated fibers acted as barriers to the matrix and increased the char yield, thus reducing the burning rate. The cone calorimeter data showed that the THR and p-HRR were significantly decreased upon the addition of nanoclays and fibers to the Epoxy/UP system. Morphology of the impact fractured samples indicates better adhesion at the fiber and matrix interface.

ACKNOWLEDGMENTS

The authors acknowledge the financial support under Center of Excellence for Green Transportation Network (CoE-GREET) sponsored by Department of Chemicals and Petrochemicals, Govt. of India.

REFERENCES

1. Reddy, P. N.; Mohanty, S.; Nayak, S. K. *Polym. Plast. Technol. Eng.* **2014**, *53*, 1723.
2. Masatoshi, K. U.; Terence, P. T.; Yoshinobu, S. Polymer Composite; Sabu, T.; Kuruvilla, J.; Malhotra, S. K.; Koichi, G.; Sreekala, M. S., Eds.; Bio fiber-Reinforced Thermoset Composites, Wiley: New York, **2014**; Vol. 3, Chapter 6, pp 213–237.
3. Satyanarayana, K. G.; Arizaga, G. G. C.; Wypych, F. *Prog. Polym. Sci.* **2009**, *34*, 982.
4. Salit, M. S. Tropical Natural Fibre Composites, Engineering Materials; Springer: Singapore, **2014**; Chapter 2, pp 15–38.
5. Mohd, A. K.; Guru, S.; Padmakaran, P.; Mishra, D.; Mudgal, M.; Dhakad, S. *J. Comp. Interf.* **2011**, *18*, 527.
6. Sreekumar, P. A.; Selvin, P. T.; Jean, M. S.; Kuruvilla, J.; Unnikrishnan, G.; Sabu, T. *Comp: Part A* **2009**, *40*, 1777.
7. Mohan, T. P.; Kanny, K. *Compos: Part A* **2012**, *43*, 1989.
8. Yan, L.; Yiu-Wing, M.; Lin, Y. *Compos. Interf.* **2005**, *12*, 141.
9. Sreekumar, P. A.; Kuruvilla, J.; Unnikrishnan, G.; Sabu, T. *Polym. Compos.* **2011**, *32*, 131.
10. Kuruvilla, J.; Romildo, D. T. F.; Beena, J.; Sabu, T.; Laura, H. de. C. *Revista. Brasileira. de Engenharia. Agrícolae. Ambiental.* **1999**, *3*, 367.
11. Yan, L.; Yiu-Wing, M. *The. J. Adhes.* **2006**, *82*, 527.
12. Xue, L.; Tabil, L. G.; Satyanarayan, P. *J. Polym. Environ.* **2007**, *15*, 25.
13. Mishra, S.; Misra, M.; Tripathy, S. S.; Nayak, S. K.; Mohanty, A. K. *Polym. Comp.* **2002**, *23*, 164.
14. Donghwan, C.; Hyun-Joong, K.; Lawrence, T. D. Polymer Composite; Sabu, T.; Kuruvilla, J.; Malhotra, S. K.; Koichi, G.; Sreekala, M. S., Eds.; Surface Treatment and Characterization of Natural Fibers: Effects on the Properties of Biocomposites, Wiley: New York, **2014**; Vol. 3, Chapter 4, pp 133–177.
15. Hamideh, H.; Mohini, S.; Lucia, H. M. *J. Nat. Fib.* **2014**, *11*, 144.
16. Augustine, P.; Kuruvilla, J.; Sabu, T. *Comp. Sci. Technol.* **1997**, *57*, 67.
17. Yan, L. *Mater. Manuf. Proc.* **2006**, *21*, 181.
18. Hongbo, G.; Jiang, G.; Qingliang, H.; Sruthi, T.; Zhang,X.; Xingru, Y.; Yudong, H.; Henry, A. C.; Suying, W.; Zhanhu, G. *Ind. Eng. Chem. Res.* **2013**, *52*, 7718.
19. Edward, M. P. Epoxy Adhesive Formulations; McGRAW-HILL: New York, **2006**.
20. Tie, L.; Gunter, B. Thermally Stable and Flame Retardant Polymer Nanocomposites; Mittal, V., Eds.; Cambridge University press: Cambridge, **2011**; Chapter 7, pp 161–185.
21. Abdelghani, L.; Jose-marie, L. Thermally Stable and Flame Retardant Polymer Nanocomposites; Mittal, V., Eds.; Cambridge University Press: Cambridge, **2011**; Chapter 12, pp 314–331.

22. Jin, U. H.; Marino, X. Thermally stable and flame retardant polymer nanocomposites; Mittal, V., Eds.; Cambridge University Press: Cambridge, **2011**; Chapter 6, pp 143–158.
23. Xiaodong, Q.; Lei, S.; Yuan, H.; Richard, K. K. Y.; Lijuan, C.; Yuqiang, G.; Ningning, H.; Saihua, J. *Ind. Eng. Chem. Res.* **2011**, *50*, 1881.
24. Xiaodong, Q.; Lei, S.; Yuan, B.; Bin, Y.; Yongqian, S.; Yuan, H.; Richard, K. K. Y. *Mater. Chem. Phys.* **2014**, *143*, 1243.
25. Aravind, D.; Zhong-Zhen, Y.; Gui-Peng, C.; Yiu-Wing, M. *Prog. Polym. Sci.* **2013**, *38*, 1357.
26. Shuyu, L.; Matthias, N. N.; Sabyasachi, G. *Prog. Org. Coat.* **2013**, *76*, 1642.
27. Muriel, R.; Michael, C.; Thomas, Z.; Manfred, D. *Phos. Sulp. Si.* **2011**, *186*, 989.
28. Lin, C. H.; Wang, C. S. *Polymer* **2001**, *42*, 1869.
29. Wang, C. S.; Lee, M. C. *Polymer* **2000**, *41*, 3631.
30. Qiang, L.; Jian-Qian, H.; Ming-Jun, C.; Jing, Z.; Yi, T.; Li, C.; Yu-ZW. *Ind. Eng. Chem. Res.* **2013**, *52*, 9397.
31. Mauro, Z. Flame Retardant Polymer Nanocomposites; Alexander, B. M.; Charles, A. W., Eds.; Wiley: New York, **2007**; Chapter 9, pp 235–284.
32. Jae-Jun, P. *Trans. Electric. Electron. Mater.* **2012**, *13*, 204.
33. Chow, W. S.; Neoh, S. S. *Polym. Plast. Technol. Eng.* **2010**, *49*, 62.
34. Islama, M. A.; Pickering, K. L.; Foreman, N. J. *J. Adhes. Sci. Technol.* **2009**, *23*, 2085.
35. Sudhakara, P.; Kannan, P.; Obireddy, K.; Rajulu, A. V. *J. Mater. Sci.* **2011**, *46*, 2778.
36. Lorena, S.; Rafael, M. E.; Clara, M. G. *Compos. Interf.* **2009**, *16*, 157.
37. Xinqi, L.; Liping, H.; Haiye, Z.; Wenjun, L.; Wenke, Z. *Carbohydr. Polym.* **2012**, *87*, 2000.
38. Pickering, K. L.; Beckermann, G. W.; Alam, S. N.; Foreman, N. *J. Compos: Part A* **2007**, *38*, 461.
39. Asumani, O. M. L.; Reid, R. G.; Paskaramoorthy, R. *Compos. Part A* **2012**, *43*, 1431.
40. Bledzki, A. K.; Gassan, J. *Prog. Polym. Sci.* **1999**, *24*, 221.
41. Weiping, L.; Hoa, S. V.; Pugh, M. *Compos. Sci. Technol.* **2008**, *68*, 2066.
42. Nikhil, G.; Tien, C. L.; Michael, S. *Nanocompos. Mater.* **2007**, 61.
43. Chinnakkannu, K. C.; Alagar, M.; Rajkumar, J. S.; Periyannan, G. *J. Polym. Res.* **2007**, *14*, 319.
44. Athijayamani, A.; Thiruchitrambalam, M.; Natarajan, U. *Polym. Compos.* **2010**, *31*, 723.
45. Piedad, G. *Polym. Compos.* **2005**, *26*, 121.
46. Chakradhar, K. V. P.; Venkata, S. K.; Ashok, K. M. *Polym. Plast. Technol. Eng.* **2012**, *51*, 92.
47. Shanmugharaj, A. M.; Sung, H. R. *Thermochim. Acta* **2012**, *546*, 16.
48. Subita, B.; Pardeep, K. V. *Int. J. Eng. Res. Technol.* **2013**, *2*, 2.
49. Worzakowska, M. *J. Appl. Polym. Sci.* **2008**, *110*, 3582.
50. Goran, N.; Sasa, Z.; Milorad, C. *Sensors.* **2010**, *10*, 684.
51. Padmavathi, T.; Naidu, S. V.; Rao, R. M. V. G. K. *J. Reinf. Plast. Compos.* **2012**, *31*, 519.
52. Rajulu, A. V.; Devi, L. G.; Rao, G. B. *J. Appl. Polym. Sci.* **2003**, *89*, 2970.
53. Kaushik, A.; Ahuja, V.; Salwani. *Compos: Part A* **2011**, *42*, 1534.
54. Chan, M. L.; Lau, K. t.; Wonga, T. T.; Cardona, F. *Appl. Surf. Sci.* **2011**, *258*, 860.
55. Ahmad, S.; Gupta, A. P.; Sharmin, E.; Alam, M.; Pandey, S. K. *Prog. Org. Coat.* **2005**, *54*, 248.
56. Taylan, E.; Kusefoglu, S. H. *J. Appl. Polym. Sci.* **2009**, *112*, 1184.
57. Poorabdollah, M.; Beheshty, M. H. *Iran. Polym. J.* **2013**, *22*, 385.
58. Shih, Y. F.; Jeng, R.-J. *Polym. Int.* **2004**, *53*, 1892.
59. Arumugam, T.; Kichenaradjou, P.; Nagarathnam, R. M. *Polym. Plast. Technol. Eng.* **2012**, *51*, 1403.
60. Jin-Chein, L.; Chang, L. C.; Nien, M. H.; Ho, H. L. *Compos. Struct.* **2006**, *74*, 30.
61. Bin, C.; Jia, L.; Haibin, C.; Jingshen, W. *Chem. Mater.* **2004**, *16*, 4864.
62. Derrick, D.; Ralph, W.; Merlin, T.; Edwin, H.; Elijah, N. *Polym.* **2005**, *46*, 3014.
63. Chang, L. N.; Chow, W. S. *J. Compos. Mater.* **2010**, *44*, 1421.
64. Ricky, S. C. W.; Yanghai, C.; Honggang, Z.; Jing, L.; Jang-Kyo, K.; Christopher, K. Y. L. *Compos. Sci. Technol.* **2007**, *67*, 3448.
65. Rawaa, A. S.; Riadh, A. M.; George, P. S.; Jana, H. *Construct. Build. Mater.* **2012**, *28*, 769.
66. Tsz-ting, W.; Kin-tak, L.; Wai-yin, T.; Jinsong, L.; Julie, A. E. *Mater. Des.* **2014**, *56*, 254.
67. Francisco, W. S.; Marcelo, J. S.; Isadora, R. N. O.; Andre, G. O.; Rivelino, M. C.; Pierre, B. A. F.; Vicente, O. S. N.; Denis, D. K.; Ronaldo, F. N. *J. Environ. Manage.* **2009**, *90*, 3340.
68. Barreto, A. C. H.; Rosa, D. S.; Fechine, P. B. A.; Mazzett, S. E. *Compos: Part A* **2011**, *42*, 492.
69. Tianxi, L.; Wuiwui, C. T.; Yuejin, T.; Chaobin, H.; Sok, S. G.; Tai-Shung, C. *J. Appl. Polym. Sci.* **2004**, *94*, 1236.
70. Darwin, P. R. K.; Gordon, S.; Monica, G. B.; Andrew, N. B. *J. Macromol. Sci. Part B: Phys.* **2005**, *44*, 1021.
71. Alamri, H.; Low, I. M.; Alothman, Z. *Compos: Part B* **2012**, *43*, 2762.
72. Viswanath, G. R.; Thangaraj, R.; Guhanathan, S. *Int. J. Polym. Anal. Charact.* **2009**, *14*, 493.
73. Al-Qadhi, M.; Merah, N.; Gasem, Z. M. *J. Mater. Sci.* **2013**, *48*, 3798.
74. Jungang, G.; Chaojie, J.; Xuejian, Z. *Int. J. Polym. Mater.* **2007**, *56*, 65.
75. Meenakshi, S.; Pradeep, J. S.; Ananda, K. S.; Umapathy, M. J. *Silicon.* **2011**, *3*, 45.
76. Lianli, D.; Minmin, S.; Jing, Y.; Kun, W.; Chengyong, H. *Ind. Eng. Chem. Res.* **2012**, *51*, 8178.
77. Wenchao, Z.; Xiangmei, L.; Rongjie, Y. *Polym. Degrad. Stab.* **2011**, *96*, 2167.

78. Wenchao, Z.; Xiangmei, L.; Haibo, F.; Rongjie, Y. *Polym. Degrad. Stab.* **2012**, *97*, 2241.

79. Kun, W.; Min-Min, S.; Yuan, H.; Weiyi, X.; Xin, W. *J. Therm. Anal. Calorim.* **2011**, *104*, 1083.

80. Kun, W.; Lei, S.; Yuan, H.; Hongdian, L.; Baljinder, K. K.; Everson, K. *Prog. Org. Coat.* **2009**, *65*, 490.

81. Quiévy, N.; Jacquet, N.; Sclavons, M.; Deroanne, C.; Paquot, M.; Devaux, J. *Polym. Degrad. Stab.* **2010**, *95*, 306.

82. Lujan-Acosta, R.; Sánchez-Valdes, S.; Ramírez-Vargas, E.; Ramos-DeValle, L. F.; Espinoza-Martinez, A. B.; Rodriguez-Fernandez, O. S.; Lozano-Ramirez, T.; Lafleur, P. G. *Mater. Chem. Phys.* **2014**, *146*, 437.

83. Maria, A. C.; Manuela, Z.; Milagros, C.; Agurtzane, M. *Polym. Degrad. Stab.* **2013**, *98*, 818.

84. Thirumal, M.; Dipak, K.; Nikhil, K. S.; Manjunath, B. S.; Naik, Y. P. J. *Macromol. Sci., Part A: Pure. Appl. Chem.* **2009**, *46*, 704.

85. Xiaodong, Q.; Lei, S.; Yuan, B.; Bin, Y.; Yongqian, S.; Yuan, H.; Richard, K. K. Y. *Mater. Chem. Phys.* **2014**, *143*, 1243.

86. Bikiaris, D. *Thermochim. Acta* **2011**, *523*, 25.

87. Singh, B.; Gupta, M.; Verma, A. *Polym. Compos.* **1996**, *6*, 910.

88. Ghosh, S.; Datta, C. *J. Mater. Sci.* **1990**, *25*, 4415.

89. Abenojar, J.; MartiNez, M. A.; Pantoja, M.; Velasco, F.; Del Real, J. C. *J. Adhes.* **2012**, *88*, 418.

90. Ming, G.; Weihong, W.; Zhi-qiang, X. *J. Appl. Polym. Sci.* **2013**, *127*, 1842.

91. Xiaodong, Q.; Lei, S.; Bin, Y.; Bibo, W.; Bihe, Y.; Yongqian, S.; Yuan, H.; Richard, K. K. Y. *J. Mater. Chem. A* **2013**, *1*, 6822.

92. Zhi-Sheng, L.; Jin-Gang, L.; Tao, S.; Deng-Xiong, S.; Shi-Yong, Y. *J. Appl. Polym. Sci.* **2014**, *131*, 40412.